

Structure, growth, and magnetism of Mn on Cu(110)

Ch. Ross, B. Schirmer, and M. Wuttig

Institut für Grenzflächenforschung und Vakuumphysik, Forschungszentrum Jülich, D-52425 Jülich, Federal Republic of Germany

Y. Gauthier

Laboratoire de Cristallographie, CNRS, Boîte Postale 166, 38042 Grenoble Cedex 9, France

G. Bihlmayer* and S. Blügel†

Institut für Festkörperforschung, Forschungszentrum Jülich, D-52425 Jülich, Federal Republic of Germany

(Received 13 June 1997; revised manuscript received 1 August 1997)

We found a two-dimensional, ordered surface alloy Cu(110)- $c(2\times 2)$ -Mn. The structure and composition of this surface compound were determined by quantitative low-energy electron-diffraction (LEED) analysis, which shows a large buckling in the surface alloy layer. The Mn atoms buckle outwards, and the Cu atoms inwards with a total buckling amplitude of 0.22 Å [17.2% of the ideal interlayer distance of Cu(110)]. The results are compared to *ab initio* total-energy and force calculations. The first-principles structure optimizations are restricted to structural relaxations normal to surface, which is consistent with our LEED analysis. The theoretically determined buckling of 16.3% reproduces the experimental situation. The calculations predict a large magnetic moment for Mn of $M=3.82\mu_B$. A hypothetical nonmagnetic Cu(110)- $c(2\times 2)$ -Mn surface alloy shows no buckling (<1%), proving that the buckling is due to the magnetovolume effect of Mn. Investigation of the growth shows that, for substrate temperatures above 180 K, deposition of submonolayer amount of Mn leads to the formation of a $c(2\times 2)$ superstructure. A well-ordered structure at 0.5 ML was observed in the temperature range between 270 and 350 K. For films above 1 ML, a 16×1 superstructure was observed giving evidence of a buckled, Mn-rich top layer. We also investigated the work-function change upon surface alloy formation. The *ab initio* calculations predict a work-function lowering of about 0.5 eV, and we identified the magnetism of Mn as the basic origin of the work-function change. The results are compared to the Cu(100)- $c(2\times 2)$ -Mn surface alloy. [S0163-1829(97)06044-X]

I. INTRODUCTION

Surface alloying after deposition of one metal onto another has gained increasing interest in the last few years.¹ This was partly motivated by the desire to tailor the properties of metallic surfaces through intermixing in the near-surface region. Furthermore, understanding the mechanisms that are invoked in surface alloying might help to achieve better control of the chemical composition profile of metallic multilayers produced by molecular-beam epitaxy or related techniques. Most studies so far have focused on the structure of surface alloys. Surprising results include the observation of surface alloying even for some metal-metal combinations which are practically immiscible in the bulk.²⁻⁷ Much less is known about the atomic mechanisms which control surface alloying.⁸

In a recent work⁹ we suggested an interesting class of surface alloys: the magnetically stabilized surface alloys. The stability of this type of alloy is due to the formation of a large magnetic moment of one type of constituent atoms of the surface alloy.

In a series of investigations, we studied the alloys formed after deposition of Mn on Cu(100) (Refs. 10–12) and Mn on Ni(100).¹³ Particular attention was devoted to the formation of ordered Cu(100)- $c(2\times 2)$ -Mn and Ni(100)- $c(2\times 2)$ -Mn surface alloys, which are characterized by a considerable atomic corrugation in the ordered surface alloy layer. Interestingly enough, no ordered bulk alloy exists for the Cu-Mn

system. Total-energy calculations have shown that the corrugation,^{9,14} stability, and formation¹⁵⁻¹⁷ of the Cu(100)- $c(2\times 2)$ -Mn surface alloy layer are due to the formation of a large magnetic moment of the Mn atoms. Several recent experiments confirmed the formation of these ordered surface alloys^{18,19} as well as the formation of these large magnetic moments.²⁰⁻²⁶

Until now, magnetically stabilized surface alloys have been investigated only at (100) surfaces. Magnetism, and also the kinetics and surface chemistry, are quantities which depend strongly on coordination number, symmetry, and the surface orientation. Thus the existence, formation, and properties of this type of surface alloy at other surfaces is unclear and unknown. To reveal the systematics that govern surface alloying for Mn on Cu single crystal surfaces, we studied the deposition of Mn on Cu(110).

In this paper we give evidence of the formation of a two-dimensional, ordered, 1-ML-thick $c(2\times 2)$ MnCu surface alloy film on Cu(110). We characterize the growth, structure, and composition of Mn films by a variety of techniques including low-energy electron diffraction (LEED), medium-energy electron diffraction (MEED), and Auger electron spectroscopy (AES). This alloy starts to form at 180-K and 0.25-ML coverage, and is stable upon cooling to 120 K and annealing to 400 K. We apply full dynamical LEED calculations to establish the structural model and the chemical composition, and to determine the atom positions. We find that the Cu and Mn film atoms show a large buckling of

17.2% of the ideal interlayer distance of Cu(110). The results are compared to *ab initio* total energy and force calculations, which reproduce the buckling of the Mn and Cu surface alloy film, and identify the magnetism as the driving force of the buckling. We predict a large magnetic moment for Mn of $M = 3.82\mu_B$. In this paper we show results on the kinetics of the alloy formation. We predict a work-function lowering of the Cu(110) work function due to alloying. We also investigate the coverage dependence of the alloy formation and observe a 16×1 superstructure at 1-ML coverage.

The formation of the Cu(110)- $c(2 \times 2)$ -Mn surface alloy is even more surprising than the formation of the Cu(100)- $c(2 \times 2)$ -Mn alloy. For the latter, one could still argue that this surface alloy may be derived from a yet unknown Cu_3Mn bulk phase, with Cu and Mn atoms arranged as in the Cu_3Au structure,²⁷ which has been speculated on in the past. This derivation does not work for the (110) face, since here the stacking of the Cu and Mn atoms are consistent with a surface plane of a Cu_3Mn bulk phase in the TiAl_3 structure. Thus the observation of the Cu(110)- $c(2 \times 2)$ -Mn phase extinguishes this kind of speculation. Moreover, it proves that the surface alloy is indeed a class of material which cannot be derived simply from bulk properties.

The paper is organized as follows. In Sec. II the experimental setup and the theoretical and computational details, respectively, are described. The results of the structure analysis, the total-energy calculations, and the magnetism are discussed in Sec. III. We close with a short summary in Sec. IV.

II. EXPERIMENTAL AND COMPUTATIONAL METHODS

A. Experiment

The experiments were performed in an UHV (ultrahigh vacuum) chamber with a base pressure of 5×10^{-9} Pa as measured by an ionization gauge. A quadrupole mass spectrometer was employed to determine the partial pressure of the residual gas, which typically consists of about 40% H_2 , 30% H_2O , and 30% CO . The Cu single crystal had a diameter of 8 mm. The surface was orientated in the [110] direction to better than 0.1° . The surface was cleaned by argon-ion sputtering (0.6 kV, $0.15 \mu\text{A}/\text{cm}^2$) and subsequent annealing by electron bombardment up to 820 K. Using an Auger system with cylindrical mirror analyzer, AES were recorded to check the surface cleanliness. Only the first preparation procedures required several cycles of sputtering, annealing and subsequent control by AES, until segregating amounts of C and O were below the Auger detection limit (<1 at. %). The sample temperature was measured by a NiCr/Ni thermocouple. Using liquid-nitrogen cooling, a minimum temperature of 120 K could be achieved. LEED was used as the main tool to analyze the structure of the surface. A three-grid backview LEED system was employed providing electron energies up to 500 eV. In most cases normal incidence was chosen. To precisely determine atomic positions, the intensities of a large number of diffraction spots was measured as a function of electron energy (LEED I/V curves; see Sec. III B for details). MEED enabled us to investigate the surface structure and morphology during Mn deposition.²⁸ In our experiments, 3-keV electrons impinged on the sample with a maximum angle of 5° against the surface plane. The diffracted beams were displayed on the fluo-

rescent LEED screen. Both for MEED and LEED I/V measurements, the diffraction pattern was recorded by a video camera and a personal computer with data-acquisition hardware and software. This allows the simultaneous measurement of up to eight different diffracted beams.

Manganese (purity 99.99%) was evaporated from a water-cooled Knudsen cell. The deposition parameters (oven temperature about 1200 K, pressure below 2×10^{-8} Pa) were kept constant in all experiments. By growing Mn on a Ni(100) surface and simultaneously using MEED, we determined the flux of Mn atoms generated from the oven. The intensity maxima of some diffracted beams are attributed to certain coverages as shown by Ref. 13. Assuming a sticking coefficient of 1, a flux of 2.5×10^{12} Mn atoms per $\text{cm}^2 \text{ s}$ was obtained, which was reproducible to within $\pm 3\%$. For the Cu(110) surface, this corresponds to a deposition rate of 0.12-ML Mn per minute. This is confirmed by the intensity maximum of the $c(2 \times 2)$ MEED curve (Fig. 5), showing that an ordered $c(2 \times 2)$ layer is completed after deposition of 0.5-ML Mn (see Sec. III A). In this paper, the coverage θ , given in units of ML Mn, is defined as the number of deposited Mn atoms per primitive substrate surface unit cell. Hence, at a coverage of 1-ML Mn there is one Mn atom for every Cu(110) surface atom.

B. LEED structure analysis

The LEED structure determination was performed with the same program, phase shifts (up to nine at high energy), and inner potential as used in our previous investigation of Mn films on Cu(100).¹¹ For this purpose we use the FORTRAN code of Moritz,^{29,30} which allows an automatic fit as well as a grid search of the parameters including the average concentration over the different sites of the unit cell. The quality of the agreement between experimental and theoretical spectra was assessed by means of two r factors, R_{DE} (Refs. 29 and 30) and R_p .³¹ Both criteria are used in the grid search algorithm and may be chosen equally to drive the automatic fit. The optimum parameters differ slightly ($\pm 0.01 \text{ \AA}$) depending on the choice of the r factor. The final results given below are derived from averaging the values obtained independently.

Optimized parameters. Atomic positions were optimized down to the third layer. Indeed, on pure fcc metal surfaces like Cu(110) or Ni(110), for instance, perturbations induced by the missing bonds in the top layer lead to changes in the three first interlayer spacings; beyond, the distance returns to the bulk value. In the present case, additional complexity is introduced by the presence of foreign atoms, namely, Mn, which replaces every other Cu atom in the top layer as demonstrated below. Since two chemical species occupy the lattice sites, a corrugation of the individual layers is likely. This was investigated in the first and third layers, while the second one was kept flat for symmetry reasons. Sharp $c(2 \times 2)$ spots were observed, indicative of a rather perfect chemical ordering in the surface layer. However, the composition was checked on both sites, assuming a random distribution of species to simulate disorder. This is realized by means of the average T -matrix approximation: each site is ascribed scattering properties equal to the compositional average of the partial amplitude of chemical elements.³²⁻³⁴ Since Mn diffu-

sion into the bulk may occur, we also determined the concentration of Mn atoms in the second layer, assuming a disordered alloy layer. In the course of the analysis, some attempts were made to refine the Debye temperatures, the inner potential V_0 , and absorptive potential V_i . V_0 was first considered constant (11 eV) and then replaced by an energy dependent potential $V_0 = -4 + 88 \times (E + 12)^{-1/2}$, which improves the agreement slightly. Further small improvements are found for a constant value of $V_i = 3.9$ eV rather than a variable one [$V_i = 0.85 \times (E + V_0)^{1/3}$]. Finally, the Debye temperature was optimized independently for the surface atoms (Cu and Mn) and for deeper layers (see Table II). Error bars are derived from the variance of R_P ,³¹ $\text{var}(R_P) = R_{P \text{ min}} \times (8V_i/\Delta E)^{1/2} = R_{P \text{ min}} \times 0.100$, where $\Delta E = 3160$ eV is the energy range common to the experimental and calculated $I(E)$ spectra.

C. Electronic structure calculation

To understand the surface magnetism and the surface structure of the Cu(110) $c(2 \times 2)$ Mn surface alloy (S) on the basis of the electronic structure, and in particular to shine more light on the role of magnetism on the surface structure, we performed a theoretical structure optimization of a hypothetical nonmagnetic (P) and a ferromagnetic (F) Cu(110) $c(2 \times 2)$ Mn surface alloy by *ab initio* electronic structure calculations. These calculations are based on the density-functional theory in the local-spin-density approximation.³⁵ The equations are solved using the full-potential linearized augmented plane-wave method (FLAPW) for thin-film geometry.³⁶ Self-consistent calculations were performed for nine-layer films consisting of seven layers of Cu with two Cu atoms per layer unit cell simulating the Cu(110) substrate, and at each surface layer one Mn and one Cu atom simulating the $c(2 \times 2)$ surface alloy according to Fig. 7(b). This structural assumption was suggested from the LEED analysis below.

The theoretical structure optimization was done in two steps. At step (i) the optimization is based on a static minimization of the total energy $E_S\{P/F; \Delta z_{\text{Mn}, F/P}; \Delta z_{\text{Cu}, F/P}\}$ with respect to the configurational degrees of freedom. We included for the nonmagnetic as well as the ferromagnetic case two degrees of freedom. These were the relaxations Δz of Mn and the top Cu atom along the surface normal. Relaxations along the surface normal are sufficient, as shown by our LEED analysis. The two-dimensional total-energy surface was calculated on 16 grid points, and the optimized structure was found by searching for the minimum of the energy surface. Including two degrees of freedom was sufficient for the Cu(100) $c(2 \times 2)$ Mn surface alloy,⁹ but the Cu(110) surface has a more open structure, and subsurface relaxation turned out to be important for an accurate description of the surface structure.

Using the previous approach which is based on total-energy minimization, it becomes very quickly impractical to determine more than two structural parameters. Recently, the force method based on the approach of Ref. 37 was implemented into our FLAPW code.³⁸ Therefore, in step (ii) we refine our structure determination using the forces exerted on the atoms together with a modified Broyden-Fletcher-Goldfarb-Shano quasi-Newton scheme³⁹ to determine the

Cu(110) $c(2 \times 2)$ Mn, nonmagnetic

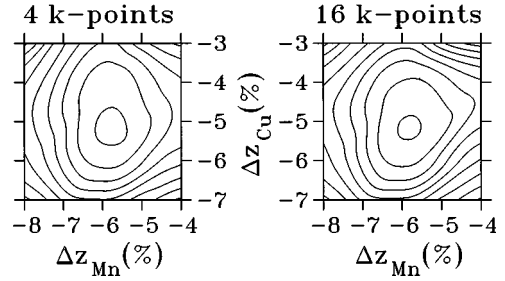


FIG. 1. Contour plots of the total-energy difference per Mn atom of nonmagnetic Cu(110) $c(2 \times 2)$ Mn with respect to the buckling relaxation Δz_{Mn} of Mn and Δz_{Cu} of the surface Cu atom. All other atoms are fixed at the ideal Cu bulk positions. The relaxations are given in relative units with respect to the theoretical interlayer spacing of Cu $d_{\text{Cu}(110)} = 1.244$ Å measured from the ideal bulk terminated surface coordinates. Calculations are carried out with four and 16 k points in the I2BZ. All other cutoff parameters are the same. The contour interval is 1 meV.

minimum-energy atomic arrangement dynamically. Further details of the method will be published elsewhere.⁴⁰

The accuracy of the calculation with respect to the two most important cutoff parameters inherent in the FLAPW method, the number of augmented plane-wave (PW) basis functions and the number of special k points in the irreducible wedge of the two-dimensional Brillouin zone (I2BZ) corresponding to the centered rectangular unit cell, have been carefully checked. In Fig. 1 we show the total energy $E_S\{P; \Delta z_{\text{Mn}}; \Delta z_{\text{Cu}}\}$ calculated for four and 16 k points in the I2BZ with little change in the calculated equilibrium position, which is $\Delta z_{\text{Mn}, P} = -5.8\%$ and $\Delta z_{\text{Cu}, P} = -5.2\%$. In Fig. 2 we show the total energy $E_S\{F; \Delta z_{\text{Mn}}; \Delta z_{\text{Cu}} = -6\%\}$ calculated for different numbers of basis functions and k points.

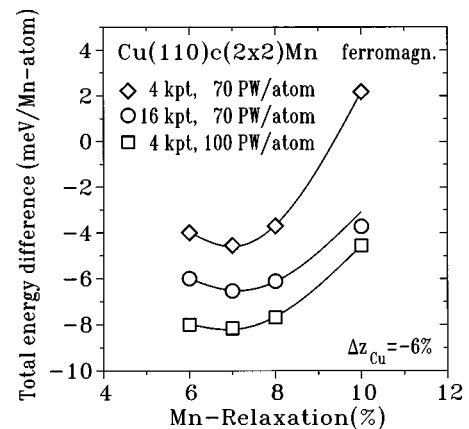


FIG. 2. Theoretical total-energy difference per Mn atom of ferromagnetic Cu(110) $c(2 \times 2)$ Mn surface alloy vs the buckling relaxation Δz_{Mn} of Mn in relative units with respect to the theoretical interlayer spacing of Cu $d_{\text{Cu}(110)} = 1.244$ Å. All Cu atoms, except the surface Cu atom, which is fixed at $\Delta z_{\text{Cu}} = -6\%$, are fixed at the ideal bulk positions. Calculations are carried out for different numbers of k points (kpt) and basis functions (PW). The origin of the energy scale is arbitrary. The equilibrium relaxation is 6.87% (4 kpt, 70 PW), 7.05% (16 kpt, 70 PW), and 6.77% (4 kpt, 100 PW).

Although the cutoff parameters chosen are too small to predict the curvature or phonon frequency of the Mn atom normal to the surface, they are sufficient for a reliable determination of the equilibrium structure of the Mn and Cu atoms in the surface layer. According to Fig. 2, the equilibrium position of the Mn atoms varies by less than 0.4% of the interlayer distance of Cu, and the magnetic moments change by $0.03\mu_B$. Throughout this paper all total-energy results presented are calculated using four \mathbf{k} points in the I2BZ and 70 PW/atom. The force calculations appear to be a bit more critical with respect to the cut-off parameters and we used 110 PW/atom and 12 \mathbf{k} points in the I2BZ. The forces were minimized down to a maximum force of 3 meV/a.u. per atom.

In addition, self-consistent calculations of the Cu(110) surface were conducted in order to compare the surface structure of the surface alloy with the plain surface, and to determine the work function change. The calculations were carried out using a $p(1\times 1)$ unit cell with one Cu atom per layer, and 36 \mathbf{k} points in the I2BZ of a rectangular unit cell. Prior to the structure determination of the surfaces of Cu(110) and Cu(110) $c(2\times 2)$ Mn, we determined the equilibrium lattice constant of bulk Cu to $a_{\text{Cu}}=3.52\text{ \AA}$ and the interlayer spacing to $d_{\text{Cu}(110)}=\sqrt{2}a_{\text{Cu}}/4=1.244\text{ \AA}$, respectively. For this purpose we used the FLAPW method in bulk geometry to avoid any incompatibilities due to different band-structure methods. The results are in fair agreement with the experimentally determined value of $d_{\text{Cu}(110)}=1.278\text{ \AA}$. All other computational parameters are equal to those used for the Cu(100) $c(2\times 2)$ Mn calculation in Refs. 9 and 15.

III. RESULTS AND DISCUSSION

In this section we present experimental results for the growth and structures of Mn on Cu(110). The atomic positions for one particular superstructure are analyzed in detail and compared with spin-dependent total-energy calculations.

A. Growth and structures of Mn on Cu(110)

After Mn deposition, two different superstructures were observed (see Fig. 3 for a survey). For substrate temperatures above 180 K, deposition of submonolayer amounts of Mn leads to the formation of a $c(2\times 2)$ superstructure. $\theta\approx 0.25\text{ ML Mn}$ is the lowest coverage producing a $c(2\times 2)$ phase. Faint and very diffuse extra spots indicate a very weak long-range order. With increasing coverage the spots become sharper and more intense, until a maximum of order and intensity is reached around $\theta=0.5\text{ ML Mn}$. Figure 4(a) shows the corresponding diffraction pattern of the ordered $c(2\times 2)$ structure at $0.50\pm 0.02\text{ ML Mn}$. If the Mn coverage exceeds 0.5-ML Mn, the $c(2\times 2)$ spots become broad and decrease in intensity, until they vanish between 1.0- and 1.5-ML Mn. The same result was obtained from MEED measurements. In Fig. 5 the intensity of a superstructure beam is plotted versus Mn coverage. Similar curves were recorded for all $c(2\times 2)$ beams, which appear and vanish simultaneously. The narrow maximum around 0.5-ML Mn confirms that this coverage corresponds to the best $c(2\times 2)$ order.

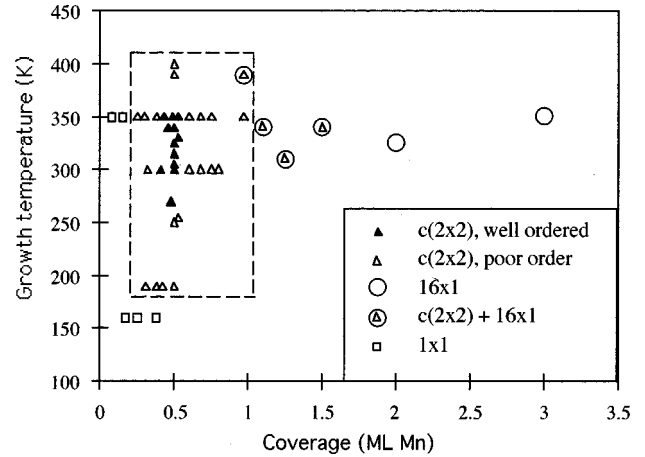


FIG. 3. Observed superstructures of Mn/Cu(110) as a function of Mn coverage (in ML Mn) and deposition temperature (in K). The broken line roughly identifies the growth region of the $c(2\times 2)$ phase.

Due to the small width of the maximum, MEED can be used for an additional coverage calibration, independent of the evaporation rate.

Figure 3 also illustrates the influence of the growth temperature on the formation of superstructures. Only in the range from about 270 K up to 350 K could a well-ordered $c(2\times 2)$ structure be observed. For lower deposition temperatures the superstructure order is considerably reduced. At 160 K, no $c(2\times 2)$ phase appears after deposition of up to 0.5-ML Mn. On the other hand, the best-ordered $c(2\times 2)$ structure was observed at temperatures as low as 120 K,⁴¹ if it was produced by deposition at 270–350 K and subsequent cooling.

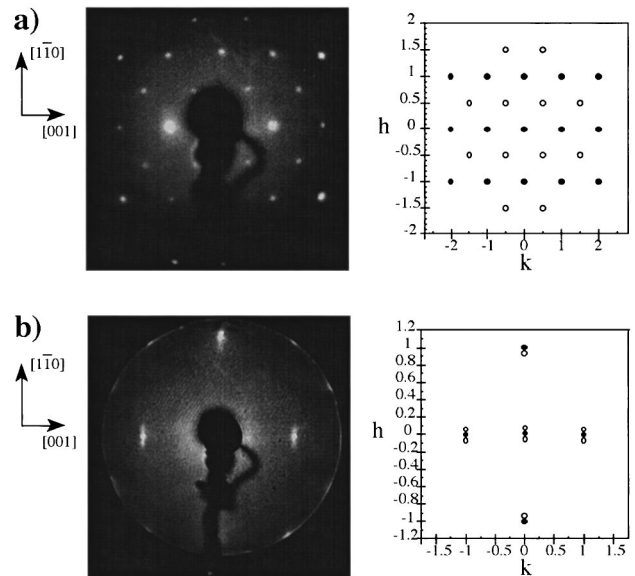


FIG. 4. LEED patterns of (a) the $c(2\times 2)$ surface alloy phase and (b) the 16×1 superstructure at electron energies of 186 and 54 eV, respectively. In (a), $0.50\pm 0.02\text{-ML Mn}$ were deposited at a sample temperature of $T=315\text{ K}$, in (b) $1.5\pm 0.05\text{ ML Mn}$ at $T=340\text{ K}$. The schematic diagrams show the positions of the substrate spots (full circles) and the extra spots of the superstructure (open circles).

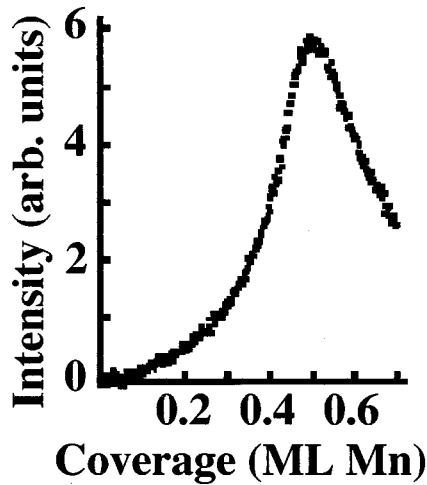


FIG. 5. Intensity of a $c(2 \times 2)$ MEED beam during Mn deposition at 300 K.

After deposition of 0.5-ML Mn at around 330 K, the substrate spots of the LEED pattern are sharp for all electron energies [see Fig. 4(a)], indicating a low density of steps. Hence, at least within the transfer width of our LEED system, which is about 80 Å, the surface is smooth and well ordered. Therefore, we suggest a two-dimensional growth mode of the $c(2 \times 2)$ superstructure up to a coverage of 0.5-ML Mn. An interesting feature of this smooth $c(2 \times 2)$ ordered layer is the presence of large domains as can be seen from the sharp extra spots in Fig. 4(a). The average domain diameter obviously exceeds the transfer width of 80 Å.

Adding Mn to the $c(2 \times 2)$ ordered surface alloy in the temperature range from 300 to 350 K, we observed a continuous phase transition towards a 16×1 superstructure (see Fig. 3). Starting with $\theta = 0.5$ ML the quality of the $c(2 \times 2)$ order decreases with increasing coverage. From 1.0- to 1.5-ML Mn, the $c(2 \times 2)$ and 16×1 phase coexist. The remaining $c(2 \times 2)$ spots are very faint and diffuse and only discernible at a few electron energies. For 2.0- and 3.0-ML Mn, the pure 16×1 phase appears in the diffraction pattern [see Fig. 4(b)]. In this phase the substrate spots are accompanied by satellite spots producing spot pairs and triplets which are elongated in the $[110]$ direction. These extra spots are sharp and intense, at least for low Miller indices (h, k) . Here the Miller index h corresponds to the $[1\bar{1}0]$ direction, k to the $[001]$ direction.

Between satellite and substrate spots there is a characteristic distance of $6.3\% \pm 0.9\%$ of the reciprocal lattice spacing in the h direction. This is the reciprocal value of 16 ± 2 . Hence the positions of the superstructure spots can be written as

$$\left(\pm \frac{1}{16}, k\right) \quad \text{and} \quad \left(\pm \frac{15}{16}, k\right) \quad (k = -2, \dots, 2).$$

These are all satellite spots which can be resolved [see Fig. 6(a)]. The observation of spots which are multiples of $\frac{1}{16}$ indicates the formation of a 16×1 superstructure, which is 16 times larger than the Cu(110) surface unit cell in the $[110]$ direction.

The characteristic feature of the observed structure is the existence of intense superstructure beams in the vicinity of

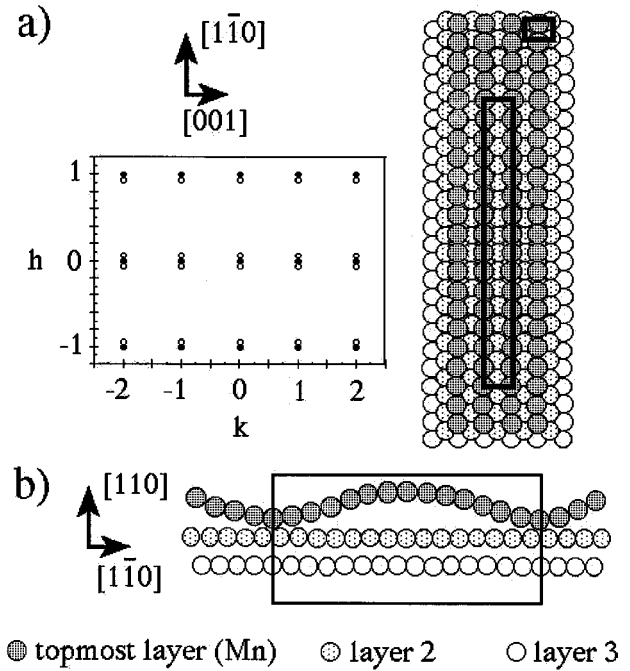


FIG. 6. (a) Schematic LEED pattern and structure model of the observed Cu(110)- (16×1) -Mn phase ($\theta \geq 1.5$ ML Mn). The LEED pattern contains the substrate spots (full circles) and all superstructure spots which could be resolved (open circles). In the model, the unit cells of the substrate (short rectangle) and the superstructure (long rectangle) are shown. (b) Side view of the model and the 16×1 unit cell. The corrugation is drastically exaggerated.

substrate beams, but the absence of other superstructure beams such as $(\frac{14}{16}, k)$, $(\frac{13}{16}, k)$, $(\frac{12}{16}, k)$, etc. The reason for this must be related to the atomic arrangement within the 16×1 unit cell. The most plausible explanation comes from a model where the scatterers in the unit cell have the spacing of $\frac{16}{15}d_{nn}$, where d_{nn} denotes the Cu nearest-neighbor distance in the $[1\bar{1}0]$ direction. This model is depicted in Fig. 6(a). The unit cell, marked by the long rectangle, consists of 16 substrate atoms with a mutual distance of d_{nn} (they may be either Cu atoms or a mixture of Cu and Mn atoms) and—as a suggestion—an adlayer of 15 Mn atoms. Additional Mn adlayers are possible for higher coverages (at least up to 3-ML Mn). This model explains the $(\pm \frac{1}{16}, k)$ spots, assuming an independent scattering of the layers. To explain the presence of $(\pm \frac{1}{16}, k)$ spots as well, one can either invoke multiple scattering between the 16×1 surface layer and the 1×1 substrate or refine the structural model further. A plausible solution for the latter approach is the assumption of a corrugated top layer as shown in Fig. 6(b). This is in line with earlier findings by Palmberg and Rhodin, who discussed the influence of an adlayer buckling for the Cu(100)- $c(10 \times 2)$ -Ag structure in some detail.^{42,43} Such modulated surface layers have recently also been found for the system Fe/Cu(100).⁴⁴ To support this model (Fig. 6), we calculated the corresponding LEED pattern for a buckled 16×1 structure on the base of the kinematic LEED theory assuming identical form factors for Mn and Cu atoms. The result is in good agreement with the observed diffraction pattern.

B. Structure determination for the Cu(110)- $c(2 \times 2)$ -Mn phase

LEED I/V measurement

After having found the optimal growth parameters for the $c(2 \times 2)$ superstructure (see Fig. 3), LEED I/V measurements were performed to enable a precise structure analysis of this phase. Four I/V data sets were recorded, each time after deposition of 0.5-ML Mn onto the substrate held at 300 K. Using the coverage calibration by MEED, the desired coverage could be achieved with an accuracy of 0.03 ML. The I/V spectra were measured at 130 K after the sample was aligned, so that the primary electron beam impinged under normal incidence. This condition was fulfilled to within $\pm 0.2^\circ$, if symmetry equivalent beams had practically identical I/V curves. Tilt and polar angles of the sample were varied, until the symmetry-equivalent beams closely matched each other. The (1,1) and (1,2) beams were measured for this purpose over the entire energy range, since these beams are most sensitive to deviations from normal incidence. Care was taken to limit both the pressure (5×10^{-9} Pa) and the time of measurement, because too high a residual gas exposure affects the $c(2 \times 2)$ structure markedly. Magnetic fields inside the chamber were reduced below 20 mG using two pairs of Helmholtz coils. Each of the four independent data sets consists of 14 nonequivalent beams: (0,1), (1,0), (1,1), (0,2), (2,0), (1,2), (2,1), (2,2), (0,3), $(\frac{1}{2}, \frac{1}{2})$, $(\frac{1}{2}, \frac{3}{2})$, $(\frac{3}{2}, \frac{1}{2})$, $(\frac{3}{2}, \frac{3}{2})$, and $(\frac{1}{2}, \frac{5}{2})$. The electron energies ranged from at least 40 eV to at most 400 eV for each beam and were varied in steps of 1 eV. The total-energy range used for the quantitative analysis amounts to 3160 eV. A visual inspection showed that the four measurements produced nearly identical I/V curves whose peak positions matched closely. To improve data quality further, symmetry-equivalent beams were averaged for the data set used in this analysis, and the intensity was normalized to constant incident current.

Structural analysis

Owing to the results derived from a related structural study of Mn/Cu(100)—Mn forms an ordered and buckled alloy surface layer with a similar $c(2 \times 2)$ periodicity¹¹—two models were investigated: a perfectly ordered surface alloy layer with the above-mentioned variations of the composition, and a pure $c(2 \times 2)$ overlayer (Fig. 7). Additionally, in the preliminary step of the analysis we also considered the possible occurrence of an ordered underlayer alloy just below the surface.

In the initial stage, varying the first two interlayer spacings and the corrugation in the Mn-Cu alloy layer when necessary, two of these models were rapidly discarded: in comparison with the surface alloy (top layer), both the alloy underlayer and the pure Mn overlayer produce high r factors and can thus be discarded, as demonstrated by the values collected in Table I. The range of variation for these parameters were sufficiently large to avoid being trapped in local minima.

We then focused on the most probable structure, the ordered Mn-Cu surface layer, including gradually variations down to the third layer. When the grid search was used, the first two interlayer spacings were always varied simultaneously with a third parameter, all others being kept fixed at

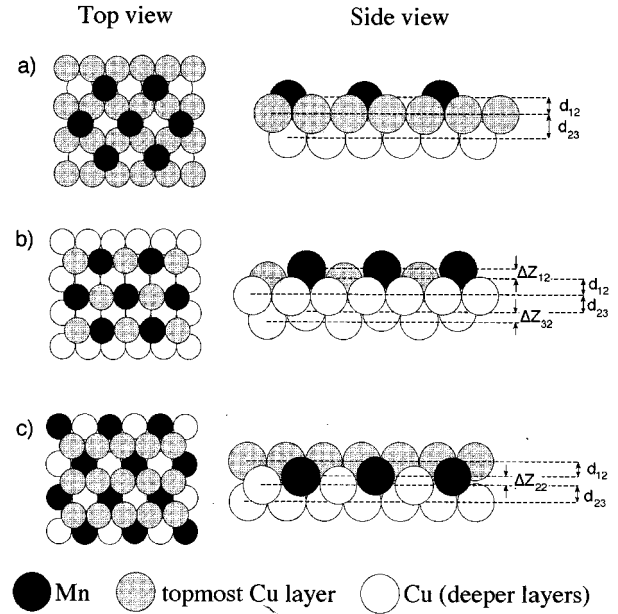


FIG. 7. Models for the Cu(110)- $c(2 \times 2)$ -Mn phase: (a) Mn overlayer, (b) Mn-Cu surface alloy (top layer), and (c) Mn-Cu alloy underlayer. The structural parameters optimized in the LEED I/V analysis are shown in the side views. ΔZ_{i2} describes the corrugation amplitude of the i th layer (height of atom 2 with respect to atom 1); d_{ij} denotes the distance from the lower atom in layer i to the highest atom in layer j .

their optimum values. The detailed results are displayed in Table II, and the changes of the r factor versus the parameters are displayed in Fig. 8. All r -factor variations are those obtained from calculations performed at the end of the analysis, fixing all parameters but one at or close to the optimum.

The coverage calibration derived from MEED measurements, together with the flux calibration, determine the coverage of the perfect $c(2 \times 2)$ structure to 0.50 ± 0.03 ML. This indicates together with the sharp $c(2 \times 2)$ superstructure spots a perfect $c(2 \times 2)$ ordered alloy where each Mn atom is surrounded by four Cu atoms, and vice versa. Therefore, we started with a model where deeper layers were assumed to be pure Cu. The buckling was refined first, looking for the chemical species (Mn or Cu) which eventually shifted outwards. The r factors do present two pronounced minima in the explored range, the lowest occurring for Mn located 0.22 \AA above the Cu sublattice. The second minimum is shifted by about 0.5 \AA , as usual with well-known periodic solutions in LEED, and corresponds to the reverse situation with Cu above the Mn sublattice. The r factors, which differ by much more than the variance ($\text{var}=0.02$) for both solu-

TABLE I. Preliminary analysis. r factors for three structural models with $c(2 \times 2)$ periodicity: Mn overlayer, ordered Mn-Cu alloy underlayer, and ordered Mn-Cu surface alloy layer (see Fig. 7).

R factor	Overlayer	Alloy underlayer	Alloy top layer
R_{DE}	0.541	0.433	0.366
R_P	0.546	0.520	0.284

TABLE II. Optimum values from automatic fit started at the minimum of the grid search. d_{ij} is defined as the distance from the lower atom in layer i to the highest atom in layer j (see Fig. 7). ΔZ_{kl} and C_{kl} are height and composition of atom l in layer k . A positive value for the buckling means that the atom is displaced inwards.

Parameter	Parameter range (grid search)	$R_{DE}=0.34$	$R_P=0.25$	Average
d_{12} (Å)	1.1–1.55	1.21	1.20	1.205 ± 0.02
d_{23} (Å)	1.13–1.38	1.28	1.30	1.29 ± 0.02
d_{34} (Å)	1.18–1.34	1.26	1.268	1.265 ± 0.02
ΔZ_{12} (Å)	–0.3–0.3	0.21	0.23	0.22 ± 0.05
ΔZ_{32} (Å)		0.01	0.01	0.01 ± 0.02
C_{11} (% Mn)	0–100	90	85	87 ± 45
C_{12} (% Cu)	0–100	92	96	94 ± 40
C_{21} (% Cu)	0–100	100	99	100 ± 35
θ_D (Mn) (K)	120–440	180	180	
θ_D (Cu _i) (K)	200–500	300	300	
θ_D (Cu _o) (K)	fixed	340	340	
ΔV_0 (eV)	0 to ± 5	–0.18	+0.16	

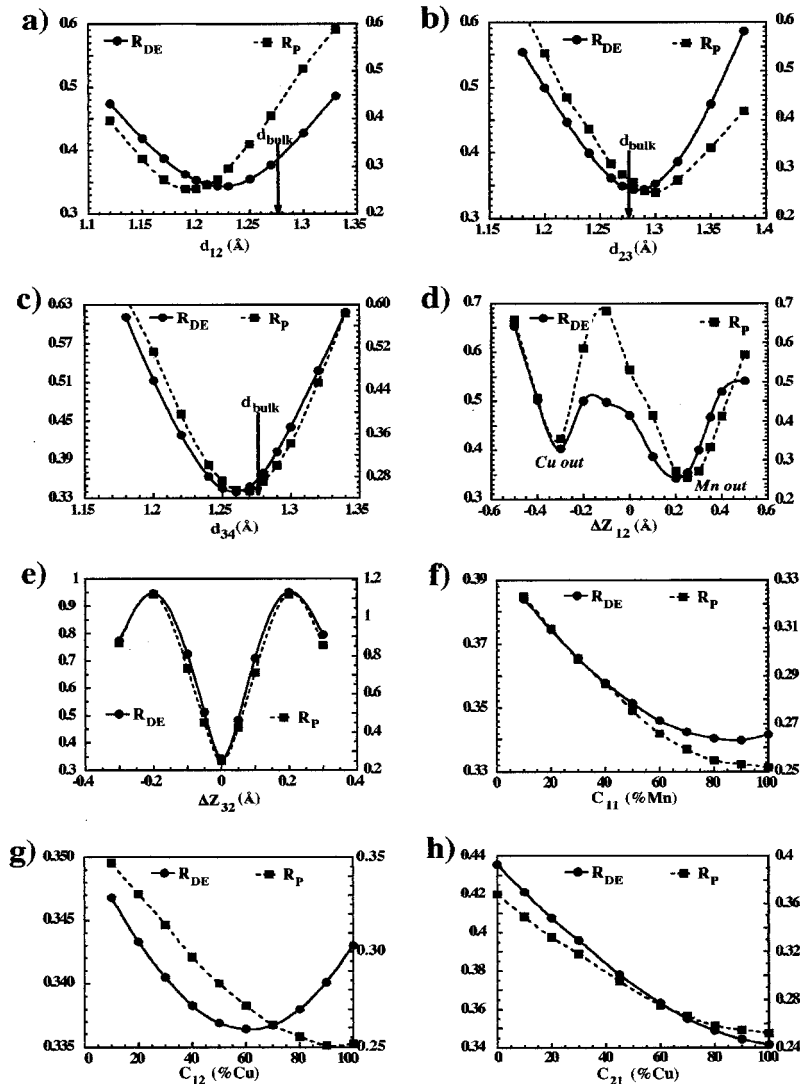


FIG. 8. Variation of r factors R_{DE} and R_P with structural and compositional parameters as scanned by grid search. d_{ij} is defined as the distance from the lower atom in layer i to the highest atom in layer j (see Fig. 7). ΔZ_{kl} and C_{kl} are the height and composition of atom l in layer k . A positive value for the buckling means that the atom is displaced inwards.

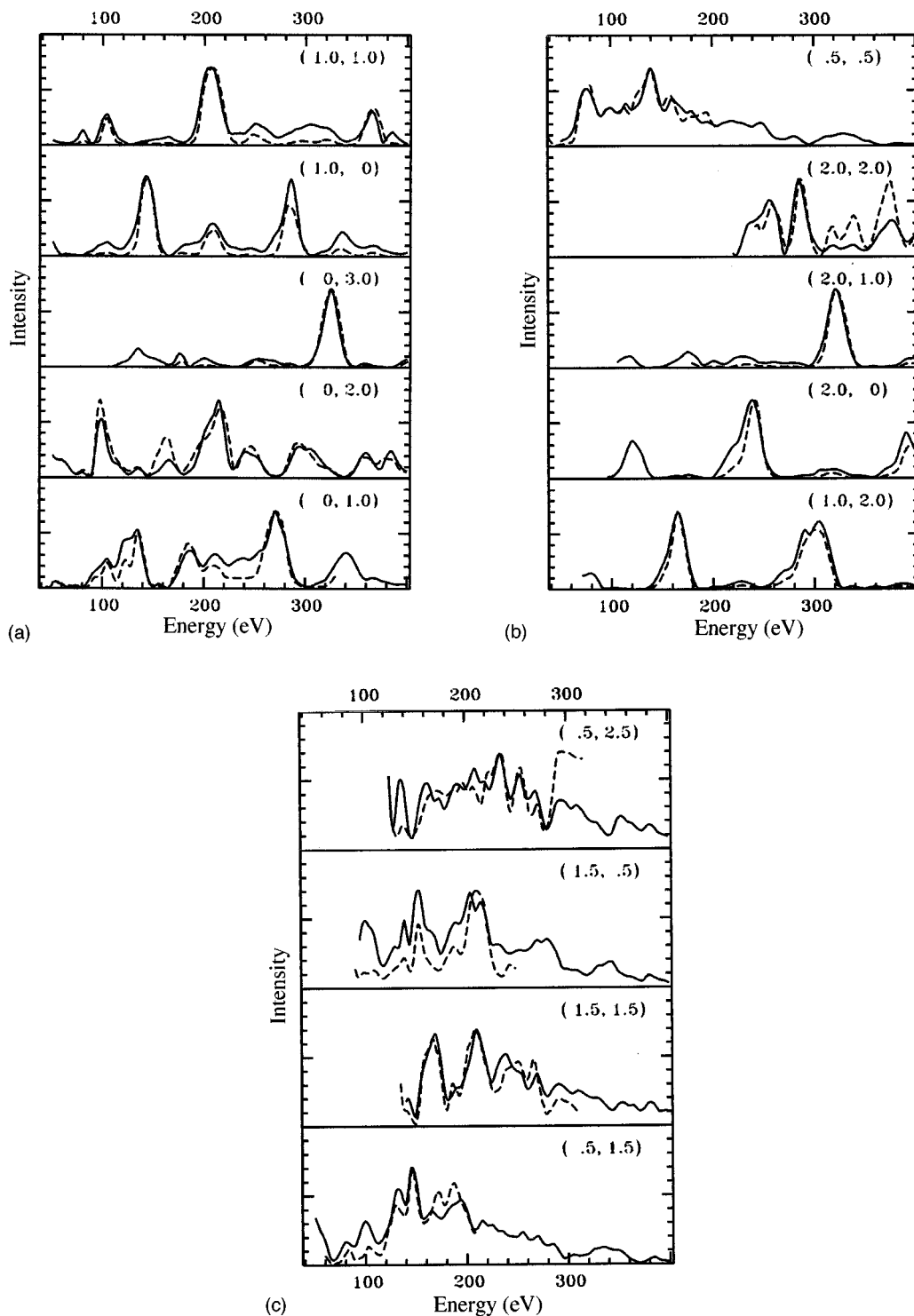


FIG. 9. LEED I/V spectra of the Cu(110)- $c(2 \times 2)$ -Mn surface alloy calculated for near-optimum parameters (solid line) in comparison to the experimental data (broken line).

tions, clearly favor the former geometry, with Mn being displaced outside.

The interlayer distance follows the general rule of fcc (110) metallic surfaces, i.e., the top Cu-Cu spacing is contracted by about 5% with respect to bulk-truncated Cu(110), whereas the second interlayer spacing is (weakly) expanded by less than 2%. We still detect some contraction in deeper layers, but it is so weak that one can consider the oscillations as almost completely damped.

As already explained, the reference structure considered so far is an ordered Mn-Cu alloy layer with a regular distribution of species so as to form a $c(2 \times 2)$ arrangement. Our experience of similar surfaces—metal on metal deposition followed by annealing to produce random or ordered alloy layers—has proven that the compositional order is seldom perfect, and that nicely ordered $c(2 \times 2)$ alloy areas may coexist with 1×1 chemically disordered domains in addition to other defects such as antiphase domain boundaries, small

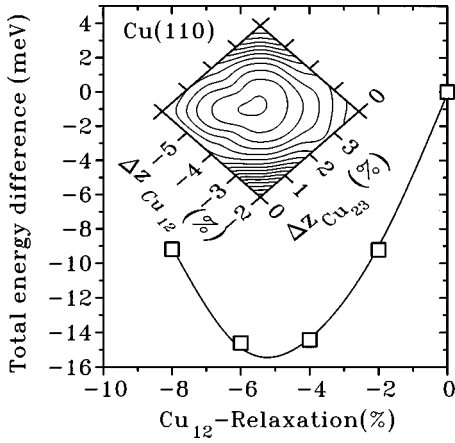


FIG. 10. Theoretical total-energy difference per Cu atom of the Cu(110) surface vs the surface-atom relaxation of $\Delta z_{\text{Cu}_{12}}$ in relative units with respect to the theoretical interlayer spacing of Cu, $d_{\text{Cu}(110)} = 1.244 \text{ \AA}$. The inset shows the contour plot including also the relaxation $\Delta z_{\text{Cu}_{23}}$ of the first subsurface Cu atoms. The minimum, which determines the optimal structure, is found in the inner circle. The contour interval is 0.5 meV. All relaxations Δz are measured from the ideal bulk-terminated surface coordinates.

islands, etc.⁴⁵ The same is likely to be true in the present instance, and we tested the possibility of a partly random distribution of Mn and Cu sites. Both sites included in the unit cell were then allowed to have an average composition at variance from the 0.5-ML Mn coverage. Besides that of the top layer, we also checked the composition of the second layer, since diffusion of Mn atoms might occur even though the temperature does not exceed room temperature during Mn deposition. The r -factor response to such variations is

shown in Fig. 8, and the optimum concentrations are given in Table II.

The error bars happen to be fairly large for the chemical composition. They are around 35 at. % in the second layer, and they even increase up to 45% for each site in the top layer. However, one should not actually be surprised by this low sensitivity: Cu and Mn are quite close in the Periodic Table of the elements, being separated by three elements only. This means that they have very similar scattering properties, which results in a weak curvature of the r factors near the minimum. Additionally, the fit concerns only half of the atoms in the top layer, which further contributes to the decrease of the sensitivity. Nevertheless the trends are far from ambiguous: both r factors exhibit a clear minimum, indicating no Mn incorporation in the second layer. For the top layer the “Mn” sublattice—shifted outward by 0.22 Å—contains almost no Cu [Fig. 8(f)], while R_{DE} points to a random mixture of 60% Cu and 40% Mn atoms on the Cu sublattice in comparison with the 90% concentration indicated by R_P as shown in Fig. 8(g). Extra confirmation of the picture is given by simultaneous automatic fit of these parameters, all others being kept fixed at their optimum: the concentrations converge close to about 94% Cu and 87% Mn respectively for the Cu and Mn sublattices, irrespective of the r factor used to drive the automatic fit. The chemical composition derived from this LEED investigation turns out to be 46% Mn and 54% Cu in the top layer (average on both sites and both r factors) which closely agrees with the coverage expected for an ideal $c(2 \times 2)$ structure (calibrated Mn flux, sharp pattern). In summary, we thus draw the conclusion that Mn and Cu form an almost perfect $c(2 \times 2)$ ordered alloy layer on top of a Mn free Cu(110) substrate.

The quality of the fit can be judged from Fig. 9 in which the experimental spectra are plotted against the theoretical

TABLE III. Survey of the results on the relaxations for the clean Cu(110) surface obtained by various techniques and authors. Δd_{ij} is the deviation of the interlayer distance between layer i and layer $j=i+1$ from the ideal bulk derived interlayer distance in relative units of the bulk interlayer distance.

Technique	Authors	Δd_{12} (%)	Δd_{23} (%)
LEED	Adams, Neilsen, and Andersen (Refs. 52 and 53)	-8.5 ± 0.6	2.3 ± 0.8
	Davis, Noonan, and Jenkins (Ref. 58)	-10.0 ± 2.5	0.0 ± 2.5
	Noonan and Davis (Ref. 55)	-8 ± 3	
	Davis and Noonan (Ref. 56)	-10.0^a	1.9
		-7.9	2.4
	-9.5	2.6	
HEIS ^b	Stensgaard and co-workers (Refs. 57 and 58)	-5.3 ± 1.6	3.3 ± 1.6
MEIS ^c	Copel <i>et al.</i> (Ref. 59)	-7.5 ± 1.5	2.5 ± 2.5
ICISS ^d	Yarmoff <i>et al.</i> (Ref. 60)	-10 ± 5	
	Fauster (Ref. 61)	-10 ± 3	8 ± 6
LEIS ^e	van de Riet <i>et al.</i> (Ref. 62)	-3 ± 3	
Theor.	Total energy ^f	-6.2	
Theor.	Force ^f	-10.2	3.8

^aDepending on the choice of the type of R -factor analysis.

^bHigh-energy ion scattering.

^cMedium-energy ion scattering.

^dImpact collision ion scattering spectroscopy.

^eLow-energy ion scattering.

^fThis work based on static total-energy minimization and force calculations.

TABLE IV. Comparison of the experimentally (LEED) and theoretically determined atom relaxations in relative units (%) of the bulk Cu(110) interlayer distance. (*P*) and (*F*) indicate nonmagnetic and ferromagnetic calculations, respectively, and energy and force indicate whether the relaxations are determined by static total-energy minimization or the use of the force method.

Technique	ΔZ_{11}	ΔZ_{31}	Δd_{12}	Δd_{23}	Δd_{34}
LEED	17.2	0.8	-5.7	0.9	-1.0
Energy (<i>P</i>)	-0.6		-5.8		
Energy (<i>F</i>)	12.7		-5.7		
Force (<i>F</i>)	16.3	3.6	-11.3	1.9	-2.2

ones for near optimum parameters. For integer as well as fractional order beams, all measured features are present in the calculated curves, and are fairly well described with very few exceptions. This is consistent with the rather good *r* factors ($R_{DE}=0.33$ and $R_p=0.25$). The remaining discrepancies are mainly the relative height of the peaks—and not the location nor the shape. The agreement is better than for the similar $c(2\times 2)$ ordered alloy which forms when 0.5-ML Mn are deposited on the Cu(100) face.¹¹

Ab initio structure optimization

Cu(110): Prior to the *ab initio* determination of the equilibrium position of the surface atoms for the unknown Cu(110)- $c(2\times 2)$ -Mn surface alloy, we compare for the plain Cu(110) surface the results of the theoretical surface Cu layer relaxation with well-known experimental data, collected in Table III. Figure 10 shows the total energy as function of the relaxation of the Cu atoms normal to the surface. Relaxing only the surface atoms, we obtain an interlayer relaxation between the surface Cu and subsurface Cu plane of $\Delta d_{12}=\Delta z_1=-5.3\%$. Including also the relaxation of the subsurface atoms, we obtain an interlayer relaxation of $\Delta d_{12}=\Delta z_1+\Delta z_2=-4.2\%-2.0\%=-6.2\%$. The energy minimization using the forces exerted on the atoms allows the determination of the multilayer relaxation of several Cu layers, and we obtain $\Delta d_{12}=-10.2\%$, $\Delta d_{23}=3.8\%$, and $\Delta d_{34}=-0.8\%$. This relaxation is accompanied by a further lowering of the total energy of 7.9 meV per surface unit cell. Comparing the theoretical results with the experimental data obtained by various experimental techniques (cf. Table III), we find overall an agreement between theory and experiments. The theoretical determination of the relaxation including only two degree of freedom as done by the static total-energy minimization leads to relaxations which are somewhat on the smaller side as compared to experiment, the dynamical structure optimization using the force exerted on the atoms leads to relaxation which are slightly on the larger side. One should take into account that the energy minimum is very shallow and energy differences of 1 meV still leads to structural changes in the range of 1%.

Cu(110)- $c(2\times 2)$ -Mn: The results of the structural optimization for the Cu(110)- $c(2\times 2)$ -Mn surface alloy are collected in Table IV together with the experimental LEED data from Sec. III A. The results of the static total-energy minimization are shown in Figs. 11(a) and 11(b). We first discuss the nonmagnetic calculations summarized in Fig. 11(a). If we allow for relaxations of the Mn and Cu surface alloy atoms, we lower the total energy by 29 meV/Mn atom, and find that their equilibrium positions, $\Delta z_{Mn,P}=-5.8\%$

and $\Delta z_{Cu,P}=-5.2\%$, are nearly identical to the relaxed atom positions of the plain Cu(110) surface, which was -5.3% , taking only the Cu surface atom into account. Thus we end up with a small buckling of about $\Delta z_{11,P}=\Delta z_{Mn,P}-\Delta z_{Cu,P}=-0.6\%$ [all relaxation given in relative

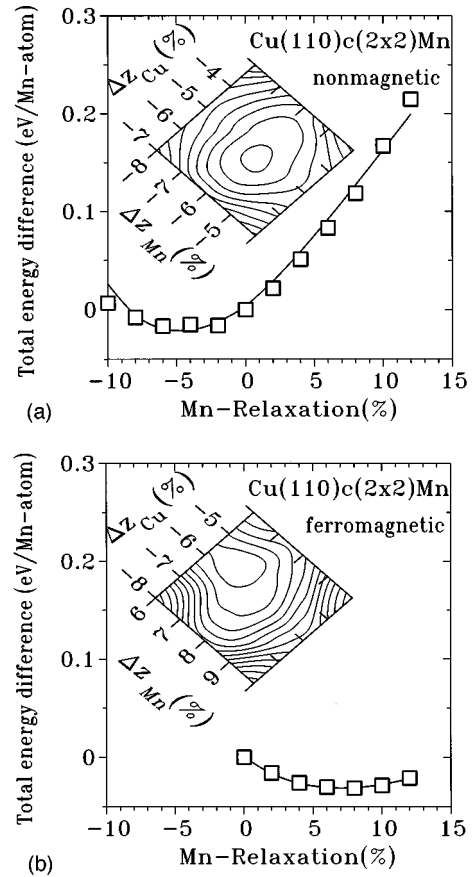


FIG. 11. Theoretical total-energy difference per Mn atom of Cu(110) $c(2\times 2)$ Mn vs the buckling relaxation Δz_{Mn} of Mn in relative units with respect to the theoretical interlayer spacing of Cu $d_{Cu(110)}=1.244$ Å. (a) and (b) shows the nonmagnetic and ferromagnetic results, respectively. The origin of the energy scale of (b) is -1.55 eV per Mn atom lower than in (a). The solid lines (surface Cu atoms fixed at the ideally terminated position $\Delta z_{Cu}=0$) are the fitting polynomials. The insets show the contour plots of the total-energy difference with respect to the buckling of Mn and Cu. The minimum, which determines the optimal structure, is found in the inner circle. The contour interval is 1 meV. All relaxations Δz are measured from the ideal bulk-terminated surface coordinates. Cu atoms, with the exception of the surface atom, are fixed at the ideal bulk positions.

units ($\Delta z/d_{\text{Cu}(110)}$ in %), where $d_{\text{Cu}(110)}$ is the ideal Cu(110) interlayer spacing]. The Mn relaxation is nearly unaffected by the relaxation of the surface Cu atom. Keeping the Cu atom at the bulk terminated position, the Mn atom relaxes by $\Delta z_{\text{Mn},P} = -5.2\%$.

When we lift the constraint of nonmagnetism and switch from a local-density calculation to a local-spin-density calculation, the system becomes magnetic, and the total energy is lowered by the magnetic energy or the spin-polarization energy, $\Delta E_{\text{sp}} = E_S(F) - E_S(P)$, respectively. The energy lowering is large and amounts to $\Delta E_{\text{sp}}(\Delta z = 0) = 1.6$ eV/Mn atom for Cu and Mn atoms at bulk-terminated atom positions. Relaxing the atomic positions of the surface Cu and Mn atoms [see Fig. 11(b)] reduces the total energy further by 51 meV. Again Cu relaxes inwards by $\Delta z_{\text{Cu},F} = -5.6\%$, but Mn relaxes outwards by $\Delta z_{\text{Mn},F} = 7.1\%$. Thus we find a large buckling in the surface alloy layer of $\Delta z_1 = \Delta z_{\text{Mn},F} - \Delta z_{\text{Cu},F} = 12.7\%$. This is in line with the large experimental buckling of 17.2% discussed above.

A closer look reveals that the relaxation of Mn does not depend much on the relaxation of the Cu surface atoms. But as we have already discussed for the ideal Cu(110) surface, additional subsurface relaxations might be important for an accurate description of the surface relaxation. Allowing the dynamical all-atom relaxations normal to the surface by force calculations, we found for the surface buckling and the third layer buckling⁴⁶ $\Delta Z_{12} = 16.3\%$ and $\Delta Z_{32} = 3.6\%$, respectively, and for the interlayer distances we obtain $\Delta d_{12} = -11.3\%$ (which is to be compared to $\Delta z_{\text{Cu},F} = -5.6\%$ without subsurface relaxation), $\Delta d_{23} = +1.9\%$, $\Delta d_{34} = -2.2\%$, and $\Delta d_{45} = +0.6\%$.

Similar results have been found for the Cu(100)-*c*(2×2)-Mn surface alloy,⁹ for which experiment and theory determined a buckling of 16.6% and 14%, respectively. Thus experiment and theory consistently found for the Cu(110)-*c*(2×2)-Mn alloy a larger buckling, speaking in relative units, and a larger spinpolarization energy E_{sp} ($E_{\text{sp,Cu}(100)} = 1.4$ eV).

Comparing theory with experiment (cf. Table IV), we can conclude that the experimental trends are well reproduced by the theory. The large buckling is in agreement with the experiment, and we can therefore conclude at this point that (i) the CuMn surface alloy is magnetic, and (ii) the buckling motion of the Mn atom is caused by the magnetism of Mn. In general, however, as for the Cu(100)-*c*(2×2)-Mn system,⁹ (i) the buckling of the surface alloy is underestimated by the theory, (ii) the relaxation of the interlayer distances Δd_{ij} are overestimated. One difference between theory and experiment is certainly the neglect of any temperature effect in the theory. The theoretical results are determined for $T = 0$ K, while the experiments are performed at 130 K. Maybe for a more accurate description one needs to go beyond the local-spin-density approximation (see also arguments below), although there is no explicit work done yet on multilayer relaxations of magnetic systems using for example the generalized gradient approximation. We consider it as a future task to shine more light onto this discrepancy.

The buckling of the CuMn layer is a nice example of a giant magneto volume effect, where the volume of the Mn atom increases with the magnetism and exerts even a pressure on the Cu surface atom, which is why

$|\Delta z_{\text{Cu},F}| > |\Delta z_{\text{Cu},P}|$. From a microscopic point of view the double occupancy of the Mn bonding states is lifted due to the magnetism, and half of the Mn bonding states are promoted to antibonding states, which make the Mn atom effectively larger and cause the large magnetobuckling effect. At the end, this volume dependence of the Mn atom on the magnetism is a complicated many-atom interaction, and therefore this buckling is very difficult to describe or predict by hard-sphere type of models with element-specific atomic radii.

C. Magnetism

Our *ab initio* calculations predict a very large magnetic moment for Mn. For the unrelaxed surface alloy a magnetic moment of $M(\Delta z = 0) = 3.77\mu_B$ was found. The buckling increases the magnetic moment to $M(\Delta z_{\text{Mn}} = 7\%, \Delta z_{\text{Cu}} = -5.7\%) = 3.82\mu_B$. Including multilayer relaxation, we find no significant change of these results. This moment is larger than for the Cu(100)-*c*(2×2)-Mn surface alloy, for which we found moments of $M(\Delta z = 0) = 3.64\mu_B$ and $M(\Delta z_{\text{Mn}} = 11.5\%, \Delta z_{\text{Cu}} = -2.5\%) = 3.75\mu_B$.⁹ We attribute this increase in the local moment of the Cu(110)-based surface alloy to the more open structure of the fcc (110) surface. At the Cu(100) surface, each surface atom has eight nearest neighbor atoms, at Cu(110), there are only seven neighbors. This reduces the hybridization, and the local magnetic moment increases (toward the atomic limit, which would be $5\mu_B$). Since Mn is already in the limit of being a strong ferromagnet,⁴⁷ and the moment is already in the saturated limit, the increase is rather small. Thus we conclude that the magnetism of Mn at the Cu(110) surface is larger than on the Cu(100) surface, which is consistent with the larger spin-polarization energy E_{sp} calculated, and the larger buckling (in relative units) of the surface alloy atoms found.

In recent experiments on the Cu(100)-*c*(2×2)-Mn surface alloys,²⁵ it was found that the intra-atomic electron correlation at the Mn atom is rather large, and the experimentally determined exchange splitting between majority and minority states is much larger than the one predicted by the local-spin-density approximation. Thus magnetism is probably underestimated by the local-spin-density approximation, which is in line with the underestimation of the surface alloy buckling. More surprising, a coverage-dependent appearance of valence-band correlation satellites was found in photoemission experiments.²⁶ These features were most pronounced for the ordered alloy, and show that the magnetism of Mn is close to the atomic limit. Since the Cu(110) surface is more open, we may speculate that the Cu(110)-*c*(2×2)-Mn surface alloy shows an even stronger satellite structure.

In this paper, we make no theoretical effort to determine the long-range magnetic order, which we assumed here to be ferromagnetic. At this point we cannot exclude the possibility of an antiferromagnetic order. It is known (cf. Ref. 48), that, for Mn monolayers on various substrates, the *c*(2×2) antiferromagnetic order is favored due to a direct in-plane Mn *d-d* hybridization. However, in the case of the CuMn surface alloy, the magnetic order is determined by an indirect, in-plane Ruderman-Kittel-Kasuya-Yosida-type interac-

TABLE V. Work functions ϕ of the relaxed and unrelaxed Cu(110) and Cu(110)- $c(2\times 2)$ -Mn surfaces in ferromagnetic (F) and (hypothetical) nonmagnetic (P) structure. The work-function changes $\Delta\phi$ upon alloying an Cu(110) surface with Mn are given for both magnetic configurations.

Cu(100)	Work function ϕ (eV)			$\Delta\phi$ (eV)	
	MnCu(110)	(P)	(F)	(P)	(F)
unrelaxed	4.88	4.75	4.46	0.13	0.42
relaxed	4.87	4.76	4.39	0.11	0.48

tion due to the hybridization of the Mn d with the Cu sp electrons. In such a case, the size of the local magnetic moment of Mn does practically not change with respect to the coupling of the moments, and since only the size of the moment causes the buckling of the surface alloy, the long-range magnetic order has practically no influence on the structural properties. Recently,⁴⁹ we calculated the $p(2\times 2)$ antiferromagnetic structure of the Cu(100)- $c(2\times 2)$ -Mn surface alloy, and found that the $p(2\times 2)$ phase is higher in energy than the $c(2\times 2)$ ferromagnetic one, and very likely the ground state of the Cu(100)- and Cu(110)- $c(2\times 2)$ -Mn surface alloys may indeed be ferromagnetic. Experimentally, the long-range order of the Cu(100)- $c(2\times 2)$ -Mn surface alloy is unknown but the upper limit of the critical temperature T_c was determined to 80 K.²⁵ In fact, also for the Cu(110)-type surface alloy, we have carefully looked for an antiferromagnetic order by LEED. As it is known, antiferromagnetism leads to extra LEED spots due to the reduced symmetry of the magnetic lattice. The intensity of fractional-order beams is estimated to be 1–2% of the primary substrate beam intensity.⁵⁰ Our LEED system, however, did not show any evidence of these. The dynamic range of this instrument allows the detection of fractional-order beams with an intensity of less than 1% of the intensity of a typical substrate beam, and the extra spots should thus be detectable.

D. Work function

In a recent work,²⁵ we made an interesting observation on the origin of the work-function change upon the alloy formation of the Cu(100)- $c(2\times 2)$ -Mn alloy at the Cu(100) surface. The first-principles calculation predicts a work-function lowering from 5.02 eV for the Cu(100) surface by 0.31 eV to 4.71 eV for the Cu(100)- $c(2\times 2)$ -Mn surface alloy, in good agreement with the experimental value of 0.45 eV. With calculations for a hypothetical nonmagnetic Cu(100)- $c(2\times 2)$ -Mn surface alloy, the work function lowering amounted to only 0.05 eV. Thus the formation of a high magnetic moment is the basic origin of a large modification of the electronic structure that causes the work-function change.

Since a large work-function change is indicative of the formation of a large magnetic moment, along this line of thought we analyzed the work-function change of Cu(110) upon the formation of the Cu(110)- $c(2\times 2)$ -Mn surface alloy (Table V). The calculated work function ϕ_{Cu} , for the unrelaxed and relaxed Cu(110) surfaces, amounts to $\phi_{\text{Cu}}(\Delta z=0)=4.88$ eV and $\phi_{\text{Cu}}(\Delta z_1=-4.2\%, \Delta z_2=2.0\%)=4.87$ eV, respectively. Upon alloy formation the work function of the unrelaxed ferromagnetic surface alloy or relaxed surface alloy lowers to $\phi_F(\Delta z=0)=4.46$ eV

or $\phi_F(\Delta z_{\text{Mn}}=7\%, \Delta z_{\text{Cu}}=-5.7\%)=4.39$ eV, respectively. Thus we obtain a work-function lowering due to the alloy formation of $\phi_F(\Delta z_{\text{Mn}}=7\%, \Delta z_{\text{Cu}}=-5.7\%) - \phi_{\text{Cu}}(\Delta z_1=-4.2\%, \Delta z_2=-2.0\%)=0.48$ eV, whereas the relaxation of the Cu and Mn atoms contributed by 0.07 eV. (Again, multilayer relaxation had no significant influence on these results.) For a hypothetical nonmagnetic Cu(110)- $c(2\times 2)$ -Mn surface alloy we predict a work function of $\phi_P(\Delta z=0)=4.75$ eV or $\phi_P(\Delta z_{\text{Mn}}=-5.8\%, \Delta z_{\text{Cu}}=-5.2\%)=4.76$ eV, respectively.

In the following we focus on the work-function change rather than on the absolute value of the work function. Using an *ab initio* method based on the local-spin-density approximation the latter is usually much less accurate. For example, we obtained for the difference between the work functions of Cu(100) and Cu(110), $\Delta\phi=0.14$ eV, close to the experimental value of 0.11 eV (cf. Ref. 51), while the absolute value of the theoretically determined work function is 0.4 eV too high as compared to the experimental value of $\phi_{\text{Cu}(110)}=4.48$ eV (cf. Ref. 51).

First, we predict that the work-function lowering due to the alloy formation is $\Delta\phi=0.11$ eV for a hypothetical nonmagnetic alloy, but $\Delta\phi=0.48$ eV for the formation of a ferromagnetic surface alloy. Thus the work-function change is even larger than for the (100) surface alloy, indicative that the effects are stronger due to the formation of a larger magnetic moment for the Cu(110)- $c(2\times 2)$ -Mn surface alloy and the more open surface. Second, for the pure Cu(110) surface and the hypothetical nonmagnetic surface alloy, the relaxation has little effect on the work function. Both surfaces remain basically smooth, but the magnetically induced buckling of the ferromagnetic surface alloy makes the surface rougher and lowers the work function by $\Delta\phi=0.06$ eV.

E. Kinetics

In Sec. III A, it was pointed out that the formation of the $c(2\times 2)$ ordered surface alloy phase starts at a deposition temperature of at least 180 K. As is known from the Mn/Cu(100) system, a minimum deposition temperature of 270 K leads to the incorporation of Mn atoms into the outermost substrate layer.^{10,11} The atomic mechanism of the formation of the Cu(100)- $c(2\times 2)$ -Mn surface alloy is the subject of current investigations.⁸ They give rise to the assumption that surface vacancies play a crucial role for Mn incorporation. If one applies this model to the Cu(110)- $c(2\times 2)$ -Mn phase, one would expect Mn incorporation at lower temperatures on Cu(110) than on the more close-packed Cu(100) surface, since the activation barrier for vacancy formation should be lower for Cu(110) than Cu(100). This is in line with the observed lower onset temperature of surface alloying for

Cu(110). However, with the present experimental data for Mn incorporation on Cu(110), other mechanisms such as an exchange process or agglomeration of Mn and Cu adatoms via intralayer mass transport cannot be excluded.

IV. SUMMARY

We found a two-dimensional, ordered surface alloy: Cu(110)- $c(2 \times 2)$ -Mn. In contrast to the previously discovered Cu(100)- $c(2 \times 2)$ -Mn phase, this surface phase cannot be derived from a presently unknown Cu_3Mn bulk phase in the Cu_3Au structure, and extinguishes this kind of speculation. It proves that the magnetic surface alloys are indeed an interesting class of material, which cannot be derived straightforward from bulk properties.

The structure and composition of this surface compound were determined by quantitative low-energy electron-diffraction analysis, which shows a large buckling in the surface alloy layer. The Mn atoms buckle outwards and the Cu atoms inwards with a total buckling amplitude of 0.22 Å [17.2% of the ideal interlayer distance of Cu(110)]. The results are compared to *ab initio* total energy and force calculations. The calculations include only the relaxations of the atoms along the surface normal, which are sufficient, as shown by our LEED analysis. The theoretically determined buckling of 16.2% reproduces the experimental situation. The calculations predict a large magnetic moment for Mn of $M = 3.82 \mu_B$. A hypothetical nonmagnetic Cu(110)- $c(2 \times 2)$ -Mn surface alloy shows no buckling (<1%), proving that the buckling is due to a large magnetovolume effect of Mn. Investigation of the growth shows that, for substrate temperatures above 180 K, deposition of submonolayer amount of Mn leads to the formation of a $c(2 \times 2)$ superstructure. A well-ordered structure at 0.5 ML was observed in the temperature range between 270 and 350 K. For films above 1 ML, a 16×1 superstructure was observed. We also investigated the work-function change upon surface-alloy formation. The *ab initio* calculations predict a work-function lowering of about 0.5 eV, and we identified the magnetism of Mn as the basic origin of the work-function change.

The results are compared to the Cu(100)- $c(2 \times 2)$ -Mn surface alloy. The buckling relaxation of the MnCu surface alloy was found, the magnetic moment and the work-function change is predicted to be larger for the Cu(110)-type surface alloy than for the Cu(100)-type surface alloy. The formation of the surface alloy was found to start at lower temperature as compared to the Cu(100)-type surface alloy, which is in line with the lower activation energy for the vacancy formation on the fcc (110) surface. We speculate that, for this more open surface, electron correlation is even more important than for the Cu(100)- $c(2 \times 2)$ -Mn system, and we expect a stronger effect on the valence-band correlation satellites in photoemission.

It would be interesting to know whether the trend on the alloy formation temperature, surface buckling, reactivity, magnetism, and work function-change from the Cu(110)- $c(2 \times 2)$ -Mn to the Cu(100)- $c(2 \times 2)$ -Mn continues to the Cu(111)- $c(2 \times 2)$ -Mn and if this phase exists at all. We hope this work also stimulates the investigation of a possible Ni(110)- $c(2 \times 2)$ -Mn for which interesting magnetic properties can be expected.

ACKNOWLEDGMENTS

This work was supported by the Deutsche Forschungsgemeinschaft (Wu 243/2). We are indebted to the DAAD for travel support within the PROCOPE program. One of us (Y.G.) is grateful to the Institut du Développement et des Ressources en Informatique Scientifique (IDRIS) for his support with computing time for the LEED calculations and is indebted to W. Moritz for providing the code. We thank T. Flores for helpful discussions, U. Linke for crystal preparation, and J. Larscheid for his technical assistance. One of us (G.B.) would like to thank the program Training and Mobility of Researchers "Interface Magnetism" (Contract: FMRX-CT96-0089) of the European Union for financial support. S.B. acknowledges support from BMBF, VDI, and a supercomputing grant "Magnetism, structure and electronic structure of ultrathin films."

*Present address: Institut für Physikalische Chemie, Universität Wien, A-1090 Wien, Austria.

†Electronic address: s.bluegel@kfa-juelich.de

¹For a collection of presently known surface alloys, see U. Bardi, Rep. Prog. Phys. **57**, 939 (1994).

²L. Pleth Nielsen, F. Besenbacher, I. Stensgaard, E. Lægsgaard, C. Engdahl, P. Stoltze, K. W. Jacobsen, and J. K. Nørskov, Phys. Rev. Lett. **71**, 754 (1993).

³H. Roder, R. Schuster, H. Brune, and K. Kern, Phys. Rev. Lett. **71**, 2086 (1993).

⁴C. Nagl, O. Haller, E. Platzgummer, M. Schmid, and P. Varga, Surf. Sci. **321**, 237 (1994).

⁵C. Nagl, E. Platzgummer, O. Haller, M. Schmid, and P. Varga, Surf. Sci. **331-333**, 831 (1995).

⁶J. Neugebauer and M. Scheffler, Phys. Rev. B **46**, 16 067 (1992).

⁷Y. Gauthier, W. Moritz, and W. Hosler, Surf. Sci. **345**, 53 (1996).

⁸M. Wuttig, T. Flores, and S. Junghans, Surf. Sci. **371**, 14 (1997).

⁹M. Wuttig, Y. Gauthier, and S. Blügel, Phys. Rev. Lett. **70**, 3619 (1993).

¹⁰T. Flores, M. Hansen, and M. Wuttig, Surf. Sci. **279**, 251 (1992).

¹¹M. Wuttig, C. C. Knight, T. Flores, and Y. Gauthier, Surf. Sci. **292**, 189 (1993).

¹²M. Wuttig, B. Feldmann, and T. Flores, Surf. Sci. **331-333**, 659 (1995).

¹³M. Wuttig, T. Flores, and C. C. Knight, Phys. Rev. B **48**, 12 082 (1993).

¹⁴M. Wuttig, S. Junghans, T. Flores, and S. Blügel, Phys. Rev. B **53**, 7551 (1996).

¹⁵S. Blügel, Appl. Phys. A: Solids Surf. **63**, 595 (1996).

¹⁶T. Asada and S. Blügel, Physica B **235-238**, 359 (1997).

¹⁷S. Blügel and T. Asada (unpublished).

¹⁸H. P. Noh, T. Hashizume, D. Jeon, Y. Kuk, H. W. Pickering, and T. Sakurai, Phys. Rev. B **50**, 2735 (1994).

¹⁹H. van Kempen and R. G. P. van der Kraan, Surf. Sci. **338**, 19 (1995).

²⁰W. L. O'Brien, J. Zhang, and B. P. Tonner, J. Phys.: Condens. Matter **5**, L515 (1993).

- ²¹W. L. O'Brien and B. P. Tonner, *J. Appl. Phys.* **76**, 6468 (1994).
- ²²W. L. O'Brien and B. P. Tonner, *Phys. Rev. B* **51**, 617 (1995).
- ²³A. B. Hayden, P. Pervan, and D. P. Woodruff, *J. Phys.: Condens. Matter* **7**, 1139 (1995).
- ²⁴D. Schmitz, O. Rader, C. Carbone, and W. Eberhardt, *Phys. Rev. B* **54**, 15 352 (1996).
- ²⁵O. Rader, W. Gudat, C. Carbone, E. Vescovo, S. Blügel, R. Kläs-ges, W. Eberhardt, M. Wuttig, J. Redinger, and F. J. Himpsel, *Phys. Rev. B* **55**, 5404 (1997).
- ²⁶O. Rader, E. Vescovo, M. Wuttig, D. D. Sarma, S. Blügel, F. J. Himpsel, A. Kimura, K. S. An, T. Mizokawa, A. Fujimori, and C. Carbone, *Phys. Rev. Lett.* (to be published).
- ²⁷The Cu₃Au structure is characterized by successive Cu(100) and *c*(2×2)-CuAu(100) planes stacked along the [100] direction. Consequently, the Cu(100)-*c*(2×2)-Mn surface alloy is a natural surface plane of Cu₃Mn bulk alloy in the Cu₃Au structure.
- ²⁸J. M. Van Hove, C. S. Lent, P. R. Pukite, and P. I. Cohen, *J. Vac. Sci. Technol. B* **1**, 741 (1983).
- ²⁹W. Moritz, H. Over, G. Kleinle, and G. Ertl, in *Proceedings IC-SOS Conference, Milwaukee, 1990*, edited by S. Y. Tong, Springer Series in Surface Sciences Vol. 24 (Springer-Verlag, Berlin, 1991), pp. 128–138.
- ³⁰G. Kleinle, W. Moritz, D. L. Adams, and G. Ertl, *Surf. Sci.* **219**, L637 (1989).
- ³¹J. B. Pendry, *J. Phys. C* **13**, 937 (1980).
- ³²Y. Gauthier, Y. Joly, R. Baudoing, and J. Rundgren, *Phys. Rev. B* **31**, 6216 (1985).
- ³³Y. Gauthier and R. Baudoing, in *Surface Segregation and Related Phenomena*, edited by P. Dowben and A. Miller (CRC, Boca Raton, 1990), pp. 169–206.
- ³⁴Y. Gauthier, in Proceedings International Workshop on "Physics and Chemistry of Alloy Surfaces" [*Surf. Rev. Lett.* **3**, 1663 (1996)].
- ³⁵U. von Barth and L. Hedin, *J. Phys. C* **5**, 1629 (1972); exchange-correlation potential in the parametrization of V. L. Moruzzi, J. F. Janak, and A. R. Williams, *Calculated Electronic Properties of Metals* (Pergamon, New York, 1978).
- ³⁶E. Wimmer, H. Krakauer, M. Weinert, and A. J. Freeman, *Phys. Rev. B* **24**, 864 (1981); M. Weinert, E. Wimmer, and A. J. Freeman, *ibid.* **26**, 4571 (1982).
- ³⁷R. Yu, D. Singh, and H. Krakauer, *Phys. Rev. B* **43**, 6411 (1991).
- ³⁸A. Di Pomponio, A. Continenza, R. Podloucky, and J. Vackar, *Phys. Rev. B* **53**, 9505 (1996).
- ³⁹D. A. H. Jacobs, in *The State of the Art of Numerical Analysis* (Academic, London, 1977).
- ⁴⁰G. Bihlmayer, S. Blügel, J. Noffke, R. Podloucky, J. Redinger, and M. Weinert (unpublished).
- ⁴¹Below 120 K, there were no results available due to use of nitrogen cooling.
- ⁴²P. W. Palmberg and T. N. Rhodin, *J. Chem. Phys.* **49**, 134 (1968).
- ⁴³P. W. Palmberg and T. N. Rhodin, *J. Chem. Phys.* **49**, 147 (1968).
- ⁴⁴S. Müller, P. Bayer, C. Reischl, K. Heinz, B. Feldmann, H. Zillgen, and M. Wuttig, *Phys. Rev. Lett.* **74**, 765 (1995).
- ⁴⁵Y. Gauthier, P. Dolle, R. Baudoing-Savois, W. Hebenstreit, E. Platzgummer, M. Schmid, and P. Varga, *Surf. Sci.* (to be published).
- ⁴⁶Second and fourth layer buckling is forbidden by symmetry.
- ⁴⁷All majority states are filled; local density of states can be found in Ref. 25.
- ⁴⁸S. Blügel, B. Drittler, R. Zeller, and P. H. Dederichs, *Appl. Phys. A: Solids Surf.* **49**, 547 (1988).
- ⁴⁹S. Blügel and M. Weinert (unpublished).
- ⁵⁰E. Tamura, S. Blügel, and R. Feder, *Solid State Commun.* **65**, 1255 (1988).
- ⁵¹J. Hölzl and F. K. Schulte, *Work Function of Metals in Solid Surface Physics* (Springer-Verlag, Berlin, 1979).
- ⁵²D. L. Adams, H. B. Nielsen, and J. N. Andersen, *Surf. Sci.* **128**, 294 (1983).
- ⁵³D. L. Adams, H. B. Nielsen, and J. N. Andersen, *Phys. Scr.* **T4**, 22 (1983).
- ⁵⁴H. L. Davis, J. R. Noonan, and L. H. Jenkins, *Surf. Sci.* **83**, 559 (1979).
- ⁵⁵J. R. Noonan and H. L. Davis, *Surf. Sci.* **99**, L424 (1980).
- ⁵⁶H. L. Davis and J. R. Noonan, *Surf. Sci.* **126**, 245 (1983).
- ⁵⁷I. Stensgaard, R. Feidenhans'l, and J. E. Sorensen, *Surf. Sci.* **128**, 281 (1983).
- ⁵⁸D. L. Adams, H. B. Nielsen, J. N. Andersen, I. Stensgaard, R. Feidenhans'l, and J. E. Sorensen, *Phys. Rev. B* **49**, 669 (1982).
- ⁵⁹M. Copel, T. Gustafsson, W. R. Graham, and S. M. Yalisove, *Phys. Rev. B* **33**, 8110 (1986).
- ⁶⁰J. A. Yarmoff, D. M. Cyr, J. H. Huang, S. Kim, and R. S. Williams, *Surf. Sci.* **165**, L73 (1986).
- ⁶¹Th. Fauster, *Vacuum* **38**, 129 (1988).
- ⁶²E. v. d. Riet, J. B. J. Smeets, J. M. Fluit, and A. Niehus, *Surf. Sci.* **214**, 111 (1989).